



Synthesis and evaluation of isoquinolinyl and pyridinyl-based dual inhibitors of fatty acid amide hydrolase and soluble epoxide hydrolase to alleviate orofacial hyperalgesia in the rat

Daniel Carr^{a,1}, Siena Gunari^{a,1}, Gabrielle Gorostiza^a, Madison Mercado^a, Lucy Pavana^a, Leah Duong^b, Karen Gomez^b, Steve Salinas^{b,} , Coral Garcia^b, Amanda Tsang^b, Christophe Morisseau^{c,} , Bruce D. Hammock^c, Stevan Pecic^{b,*,} , Ram Kandasamy^{a,*,}

^a Department of Psychology, California State University, East Bay, Hayward, CA, USA

^b Department of Chemistry and Biochemistry, California State University, Fullerton, Fullerton, CA, USA

^c Department of Entomology and Nematology and UCD Comprehensive Cancer Center, University of California, Davis, Davis, CA, USA

ARTICLE INFO

Keywords:

Polypharmacology
Formalin
Orofacial
Enzyme inhibition
Structure-activity relationship studies

ABSTRACT

The treatment of orofacial pain disorders is poor. Both opioids and serotonin agonists are commonly used; however, they produce dangerous and unpleasant side effects. Therefore, there is an urgent need to identify new pharmacological treatments that can resolve orofacial pain. Moreover, a treatment that engages multiple mechanisms using one compound may be advantageous. Fatty acid amide hydrolase (FAAH) and soluble epoxide hydrolase (sEH) are two enzymes that can regulate both pain and inflammation via independent pathways. Small molecules that inhibit both enzymes simultaneously were previously synthesized and produced antinociception *in vivo*. Quinolinyl-based dual inhibitors of FAAH and sEH can inhibit acute inflammatory pain in rats. Here, following on these findings, we generated 7 new isoquinolinyl- and 7 pyridinyl-based analogs and tested their inhibition at both enzymes. Structure-activity relationship study coupled with docking experiments, revealed that the isoquinoline moiety is well-tolerated in the binding pockets of both enzymes, yielding several analogs with nanomolar activity in enzymatic assays. All newly synthesized analogs were assessed in the solubility assay at pH 7.4, and we determined that isoquinolinyl- and substituted pyridinyl-analogs exhibit limited solubility under the experimental conditions. The most potent inhibitor, **4f**, with IC₅₀ values in the low nanomolar range for both enzymes, was evaluated in a plasma stability assay in human and rat plasma where it showed a moderate stability. Primary binding assays revealed that **4f** does not engage any opioid or serotonin receptors. A high dose (3 mg/kg) of **4f** reversed orofacial hyperalgesia following pretreatment with nitroglycerin and orofacial injection of formalin; however, this same dose did not inhibit acute orofacial inflammatory pain or restore pain-depressed wheel running. These findings indicate that simultaneous inhibition of FAAH and sEH using isoquinolinyl-based dual inhibitors may only reverse certain components of orofacial hyperalgesia.

1. Introduction

The trigeminal system plays a central role in head and face pain with peripheral and central neurons sensitized by inflammatory mediators resulting in pain in both humans and animals [1,2]. Painful stimuli within the orofacial region, such as tissue damage or administration of noxious chemicals, provokes inflammation within the nervous system

[3]. Existing treatments for orofacial pain typically target one receptor or enzyme and include prophylactic treatments such as triptans [4] which may lead to long-term effects, including medication-overuse headache [5], while nonsteroidal anti-inflammatory drugs (NSAIDs) can cause gastrointestinal issues [6]. Therefore, there is a desperate need for novel therapies to reverse orofacial pain with limited side effects.

One potential way to reverse orofacial pain is to inhibit multiple

* Corresponding author.

** Corresponding author.

E-mail addresses: specic@fullerton.edu (S. Pecic), ram.kandasamy@csueastbay.edu (R. Kandasamy).

¹ indicates equal contribution.

enzymes responsible for pain and inflammation. Soluble epoxide hydrolase (sEH) [7] and fatty acid amide hydrolase (FAAH) [8] play important roles in the modulation of pain and inflammation. Epoxide hydrolases elicit their effects through the interaction with epoxide-containing lipids and the addition of water [9]. One such epoxide-containing lipid is epoxyeicosatrienoic acid (EET). EETs play a critical role in reducing inflammation and are known to be analgesic [10]. Previous studies have shown that selective sEH inhibitors have been effective in reducing pain, lack motor function effects, and lack drug tolerance with repeated dosing in rat models [11], indicating that they may produce safe and effective pain relief. FAAH is an integral membrane enzyme that degrades the fatty acid amide family of endogenous signaling lipids [12]. This includes endogenous lipid ligands called endocannabinoids such as N-arachidonylethanolamine (anandamide; AEA) [13]. These lipid ligands activate the G-protein coupled receptors CB₁ and CB₂, which promote analgesic and anti-inflammatory effects in humans and animals [14,15]. Selective pharmacological inhibition of FAAH produces pain relief in several animal models of both acute and chronic pain (e.g., Refs. [16–18]). Importantly, selective sEH inhibition has been shown to inhibit trigeminal inflammation and pain in rats [19] and selective FAAH inhibition also inhibits trigeminal hyperalgesia in rats and mice [20–22]. Further, one study has demonstrated *enhanced* pain relief following co-administration of a sEH inhibitor and FAAH inhibitor [23], indicating a synergistic antinociceptive effect.

We have previously synthesized and evaluated several dual inhibitors of FAAH and sEH i.e. a small molecule that simultaneously inhibits both enzymes. Dual inhibitors of FAAH and sEH produce antinociception against formalin-induced hind paw inflammatory pain [24–27], and they do so at doses that do not depress voluntary activity [28]. We have also previously demonstrated that 4-phenyl-thiazole-based dual inhibitors of FAAH and sEH do not alleviate orofacial pain [29]; however, we did not evaluate whether dual FAAH/sEH inhibitors alleviate orofacial hyperalgesia.

Therefore, in this work the follow-up structure-activity relationship study was performed on our previously identified lead compound, a quinolinyl-based dual FAAH/sEH inhibitor [24] and we generated 14 new analogs, organized in two libraries, and evaluated them in enzymatic inhibition assays for both FAAH and sEH. The most potent dual inhibitor identified in this study, **4f**, was subsequently assessed in human and rat microsomal liver assays for stability, solubility assays, opioid and serotonin receptor primary binding assays, and *in vivo* against orofacial hyperalgesia in female rats. Hyperalgesia was evaluated using measures of pain-evoked [30] behaviors, and pain-depressed behaviors such as wheel running [31] were evaluated to determine the effect of **4f** on restoring pain-depressed activity in rats, a clinically relevant symptom of trigeminal pain in humans [32,33].

2. Materials and methods

2.1. Chemistry

All chemicals, including starting materials, reagents, and solvents, were sourced commercially from Sigma Aldrich, TCI and Fisher Scientific, and utilized without additional purification. Reaction progress was tracked using thin-layer chromatography (TLC) on silica gel 60 F254 precoated aluminum plates. For purification, all intermediates and final products were processed through flash chromatography using Teledyne CombiFlash Rf + Separation System, employing prepacked silica gel columns from Teledyne. The purity of the final compounds (95 % or higher) was confirmed by TLC, LC-MS, HRMS and both proton and carbon NMR. Proton and carbon NMR spectra were obtained using a Bruker Avance-II spectrometer operating at 400 MHz and 101 MHz, respectively, in either deuterated chloroform (CDCl₃) with tetramethylsilane (TMS) as an internal reference or deuterated dimethyl sulfoxide (DMSO-*d*₆). Chemical shifts (δ) are expressed in parts per million

(ppm) and coupling constants (*J*) in Hertz (Hz). Multiplicity abbreviations: s = singlet, bs = broad singlet, d = doublet, t = triplet, q = quartet, m = multiplet. LCMS analyses were conducted on a Shimadzu 2050 System using LC-grade solvents, with conditions set as follows: eluent A consisted of water with 0.05 % TFA, and eluent B of acetonitrile with 0.05 % TFA, using an isocratic gradient (5 min, A = 20 %, B = 80 %) at a flow rate of 0.4 mL/min, through a Phenomenex Kinetex 1.7 μ m C18 100 Å, 50 mm \times 2.1 mm column. Analyses were performed in positive ion mode. High-resolution liquid chromatography mass spectrometer (ThermoFisher Ultimate 3000 binary UPLC coupled to a Q Exactive Focus Orbitrap mass spectrometer) was used to confirm the masses. The elution gradient increased from acetonitrile:water (20:80 + 0.1 % formic acid) to acetonitrile:water (70:30 + 0.1 % formic acid) over 3 min and held for 1 min at a flow rate of 0.4 mL/min. Microwave-assisted reactions were executed using a CEM 2.0 Discover microwave synthesizer. Melting points were assessed using a DigiMelt MPA-160 apparatus and are reported without correction. Fatty Acid Amide Hydrolase (human, recombinant) was obtained from Cayman Chemical, while Soluble Epoxide Hydrolase (human, mouse, and rat, recombinant) was sourced from UC Davis (BDH lab). Molecular modeling and docking studies were carried out with ICM Pro Molsoft software.

2.2. General procedure for the preparation of **4a-n**

Intermediates **1**, **2**, and **3** were prepared using previously published procedures [24,27] (Supplemental 3).

A mixture of 0.198 mmol of intermediate **3**, 0.396 mmol of the appropriate bromoisoquinoline or bromopyridine, and 0.495 mmol of potassium carbonate were dissolved in a 4:1 solvent mixture of tetrahydrofuran/water. Following the addition of 0.010 mmol of palladium-tetrakis(triphenylphosphine), the reaction mixture was subjected to microwave irradiation at 110 °C for 60 min. The solvent was then evaporated under reduced pressure, and the residue was dissolved in 50 mL of DCM and 25 mL of water. The organic layer was separated, dried over anhydrous sodium sulfate, filtered, and concentrated *in vacuo*. The crude product was purified using a CombiFlash system with the following parameters: 0–50 % ethyl acetate and 100–50 % hexane over 20 min, yielding final products **4a-n** in moderate yields.

1-((2-chlorophenyl)sulfonyl)-N-(4-(isoquinolin-1-yl)phenyl)piperidine-4-carboxamide (**4a**) was obtained as a white solid in the amount of 0.082 g, (83 % yield): mp: 152–153 °C. ¹H NMR (400 MHz; DMSO-*d*₆): δ 10.13 (s, 1H), 8.54 (d, *J* = 5.6 Hz, 1H), 8.05–8.00 (m, 3H), 7.80–7.77 (m, 4H), 7.71–7.70 (m, 1H), 7.68–7.64 (m, 1H), 7.62 (t, *J* = 2.2 Hz, 2H), 7.60 (t, *J* = 1.7 Hz, 1H), 7.58–7.56 (m, 1H), 3.79–3.76 (m, 2H), 2.85 (td, *J* = 12.4, 2.3 Hz, 2H), 2.54 (s, 1H), 1.92–1.88 (m, 2H), 1.68–1.60 (m, 2H). ¹³C NMR (101 MHz, DMSO-*d*₆): δ 173.3, 159.7, 142.5, 140.0, 136.8, 136.4, 134.9, 134.3, 132.8, 132.0, 131.4, 130.80, 130.64, 128.29, 128.09, 127.6, 127.2, 126.2, 120.1, 119.2, 45.2, 42.2, 28.5. ESI-MS (*M*⁺+H): 506. HRMS-ESI+: calculated for C₂₇H₂₄ClN₃O₃S + H: 506.1305; Found: 506.1287.

1-((2-chlorophenyl)sulfonyl)-N-(4-(isoquinolin-3-yl)phenyl)piperidine-4-carboxamide (**4b**) was obtained as a white solid in the amount of 0.017 g, (17 % yield): mp: 147–150 °C. ¹H NMR (400 MHz; DMSO-*d*₆): δ 10.05 (s, 1H), 9.35 (s, 1H), 8.33 (s, 1H), 8.16–8.13 (m, 2H), 8.10–8.08 (m, 1H), 8.00–7.96 (m, 2H), 7.77–7.54 (m, 7H), 3.77–3.73 (m, 2H), 2.86–2.79 (m, 2H), 2.53–2.49 (m, 1H), 1.89–1.85 (m, 2H), 1.65–1.57 (m, 2H). ¹³C NMR (101 MHz, DMSO-*d*₆): δ 173.2, 152.7, 149.9, 140.1, 136.7, 136.3, 134.9, 134.0, 132.7, 132.0, 131.33, 131.23, 128.3, 128.0, 127.6, 127.3, 119.7, 115.5, 45.2, 42.1, 28.5. ESI-MS (*M*⁺+H): 506. HRMS-ESI+: calculated for C₂₇H₂₄ClN₃O₃S + H: 506.1305; Found: 506.1284.

1-((2-chlorophenyl)sulfonyl)-N-(4-(isoquinolin-4-yl)phenyl)piperidine-4-carboxamide (**4c**) was obtained as a white solid in the amount of 0.047 g, (47 % yield): mp: 146–148 °C. ¹H NMR (400 MHz; DMSO-*d*₆): δ 10.10 (s, 1H), 9.30 (s, 1H), 8.39 (s, 1H), 8.19 (d, *J* = 7.8 Hz, 1H), 8.00 (dd, *J* = 7.9, 1.5 Hz, 1H), 7.85 (d, *J* = 8.5 Hz, 1H), 7.76–7.52 (m, 7H),

7.46 (d, $J = 8.5$ Hz, 2H), 3.79–3.75 (m, 2H), 2.88–2.81 (m, 2H), 2.56–2.50 (m, 1H), 1.91–1.85 (m, 2H), 1.68–1.58 (m, 2H). ^{13}C NMR (101 MHz, DMSO- d_6): δ 173.3, 152.2, 142.8, 139.5, 136.4, 134.9, 133.7, 132.75, 132.59, 131.99, 131.87, 131.45, 131.35, 130.7, 129.25, 129.13, 128.5, 128.3, 127.9, 124.5, 119.7, 100.0, 45.2, 42.1, 28.5. ESI-MS ($\text{M}^+ + \text{H}$): 506. HRMS-ESI+: calculated for $\text{C}_{27}\text{H}_{24}\text{ClN}_3\text{O}_3\text{S} + \text{H}$: 506.1305; Found: 506.1286.

1-((2-chlorophenyl)sulfonyl)-N-(4-(isoquinolin-5-yl)phenyl)piperidine-4-carboxamide (**4d**) was obtained as a white solid in the amount of 0.039 g, (39 % yield): mp: 190–192 °C. ^1H NMR (400 MHz; DMSO- d_6): δ 10.09 (s, 1H), 9.40–9.35 (m, 1H), 8.49–8.45 (m, 1H), 8.12 (dd, $J = 8.2$, 3.5 Hz, 1H), 8.02–7.99 (m, 1H), 7.77–7.67 (m, 6H), 7.63–7.51 (m, 2H), 7.43 (d, $J = 8.5$ Hz, 2H), 3.79–3.73 (m, 2H), 2.88–2.80 (m, 2H), 2.57–2.50 (m, 1H), 1.91–1.85 (m, 2H), 1.69–1.57 (m, 2H). ^{13}C NMR (101 MHz, DMSO- d_6): δ 173.2, 143.8, 139.4, 138.5, 136.4, 134.9, 133.58, 133.51, 132.8, 131.99, 131.88, 131.4, 130.5, 129.25, 129.14, 129.08, 128.3, 127.64, 127.52, 119.7, 45.2, 42.1, 28.5. ESI-MS ($\text{M}^+ + \text{H}$): 506. HRMS-ESI+: calculated for $\text{C}_{27}\text{H}_{24}\text{ClN}_3\text{O}_3\text{S} + \text{H}$: 506.1305; Found: 506.1285.

1-((2-chlorophenyl)sulfonyl)-N-(4-(isoquinolin-6-yl)phenyl)piperidine-4-carboxamide (**4e**) was obtained as a white solid in the amount of 0.078 g, (78 % yield): mp: 247–249 °C. ^1H NMR (400 MHz; DMSO- d_6): δ 10.11 (s, 1H), 9.33–9.27 (m, 1H), 8.53–8.46 (m, 1H), 8.20–8.14 (m, 2H), 8.01–7.97 (m, 2H), 7.84–7.79 (m, 3H), 7.73–7.65 (m, 3H), 7.63–7.51 (m, 2H), 3.78–3.75 (m, 2H), 2.87–2.80 (m, 2H), 2.56–2.51 (m, 1H), 1.90–1.86 (m, 2H), 1.65–1.57 (m, 2H). ^{13}C NMR (101 MHz, DMSO- d_6): δ 173.2, 152.5, 143.7, 141.8, 139.9, 136.4, 136.1, 134.9, 134.1, 132.7, 132.0, 131.3, 129.24, 129.13, 128.7, 128.3, 128.0, 127.6, 126.8, 123.4, 121.0, 120.0, 45.2, 42.1, 28.5. ESI-MS ($\text{M}^+ + \text{H}$): 506. HRMS-ESI+: calculated for $\text{C}_{27}\text{H}_{24}\text{ClN}_3\text{O}_3\text{S} + \text{H}$: 506.1305; Found: 506.1283.

1-((2-chlorophenyl)sulfonyl)-N-(4-(isoquinolin-7-yl)phenyl)piperidine-4-carboxamide (**4f**) was obtained as a white solid in the amount of 0.055 g, (55 % yield): mp: 206–207 °C. ^1H NMR (400 MHz; DMSO- d_6): δ 10.10 (s, 1H), 9.39–9.34 (m, 1H), 8.48 (dd, $J = 6.7$, 4.4 Hz, 1H), 8.39–8.38 (m, 1H), 8.10 (dd, $J = 8.7$, 1.9 Hz, 1H), 8.03–7.99 (m, 2H), 7.83–7.79 (m, 2H), 7.74–7.66 (m, 4H), 7.62–7.53 (m, 2H), 3.79–3.74 (m, 2H), 2.87–2.79 (m, 2H), 2.55–2.51 (m, 1H), 1.90–1.85 (m, 2H), 1.67–1.56 (m, 2H). ^{13}C NMR (101 MHz, DMSO- d_6): δ 173.2, 153.1, 143.2, 139.6, 138.9, 136.4, 134.9, 134.6, 134.2, 132.8, 131.99, 131.87, 131.3, 129.8, 129.25, 129.14, 128.3, 127.72, 127.57, 124.5, 120.5, 120.1, 45.2, 42.1, 28.5. ESI-MS ($\text{M}^+ + \text{H}$): 506. HRMS-ESI+: calculated for $\text{C}_{27}\text{H}_{24}\text{ClN}_3\text{O}_3\text{S} + \text{H}$: 506.1305; Found: 506.1286.

1-((2-chlorophenyl)sulfonyl)-N-(4-(isoquinolin-8-yl)phenyl)piperidine-4-carboxamide (**4g**) was obtained as a white solid in the amount of 0.048 g, (48 % yield): mp: 127–130 °C. ^1H NMR (400 MHz; DMSO- d_6): δ 10.12 (s, 1H), 9.20–9.15 (m, 1H), 8.56–8.48 (m, 1H), 8.03–7.93 (m, 2H), 7.90–7.87 (m, 1H), 7.82–7.75 (m, 3H), 7.72–7.66 (m, 2H), 7.61–7.53 (m, 2H), 7.48–7.46 (m, 1H), 3.79–3.71 (m, 2H), 2.88–2.79 (m, 2H), 2.57–2.51 (m, 1H), 1.91–1.81 (m, 2H), 1.68–1.56 (m, 2H). ^{13}C NMR (101 MHz, DMSO- d_6): δ 173.3, 143.1, 140.2, 139.5, 136.36, 136.26, 135.3, 134.9, 133.7, 132.8, 131.99, 131.87, 131.4, 130.7, 129.25, 129.13, 128.7, 128.3, 126.40, 126.30, 121.1, 119.6, 45.2, 42.1, 28.5. ESI-MS ($\text{M}^+ + \text{H}$): 506. HRMS-ESI+: calculated for $\text{C}_{27}\text{H}_{24}\text{ClN}_3\text{O}_3\text{S} + \text{H}$: 506.1305; Found: 506.1285.

1-((2-chlorophenyl)sulfonyl)-N-(4-(pyridin-2-yl)phenyl)piperidine-4-carboxamide (**4h**) was obtained as a white solid in the amount of 0.055 g, (61 % yield): mp: 206–207 °C. ^1H NMR (400 MHz; DMSO- d_6): δ 10.05 (s, 1H), 8.60 (t, $J = 0.4$ Hz, 1H), 8.02–7.99 (m, 3H), 7.88 (d, $J = 7.4$ Hz, 1H), 7.81 (s, 1H), 7.67 (s, 4H), 7.57 (d, $J = 7.0$ Hz, 1H), 7.28–7.27 (m, 1H), 3.77–3.76 (m, 2H), 2.85–2.79 (m, 2H), 2.54–2.51 (m, 1H), 1.88–1.85 (m, 2H), 1.64–1.56 (m, 2H). ^{13}C NMR (101 MHz, DMSO- d_6): δ 173.2, 156.0, 149.8, 140.4, 137.6, 136.3, 134.9, 133.8, 132.7, 132.0, 131.3, 128.3, 127.3, 122.5, 120.0, 119.6, 45.2, 42.1, 28.5. ESI-MS ($\text{M}^+ + \text{H}$): 456. HRMS-ESI+: calculated for $\text{C}_{23}\text{H}_{22}\text{ClN}_3\text{O}_3\text{S} + \text{H}$: 456.1149; Found: 456.1135.

1-((2-chlorophenyl)sulfonyl)-N-(4-(pyridin-3-yl)phenyl)piperidine-

4-carboxamide (**4i**) was obtained as a white solid in the amount of 0.054 g, (60 % yield): mp: 197–200 °C. ^1H NMR (400 MHz; DMSO- d_6): δ 10.02 (s, 1H), 8.84 (t, $J = 3.4$ Hz, 1H), 8.50 (dd, $J = 4.7$, 1.5 Hz, 1H), 8.02–7.98 (m, 2H), 7.70–7.65 (m, 6H), 7.58–7.54 (m, 1H), 7.44–7.40 (m, 1H), 3.77–3.73 (m, 2H), 2.85–2.78 (m, 2H), 2.52–2.50 (m, 1H), 1.88–1.84 (m, 2H), 1.65–1.55 (m, 2H). ^{13}C NMR (101 MHz, DMSO- d_6): δ 173.2, 148.5, 147.7, 139.7, 136.3, 135.5, 134.9, 133.9, 132.7, 132.0, 131.3, 129.24, 129.13, 128.3, 127.5, 124.2, 120.05, 119.96, 45.2, 42.1, 28.5. ESI-MS ($\text{M}^+ + \text{H}$): 456. HRMS-ESI+: calculated for $\text{C}_{23}\text{H}_{22}\text{ClN}_3\text{O}_3\text{S} + \text{H}$: 456.1149; Found: 456.1128.

1-((2-chlorophenyl)sulfonyl)-N-(4-(pyridin-4-yl)phenyl)piperidine-4-carboxamide (**4j**) was obtained as a white solid in the amount of 0.051 g, (57 % yield): mp: 206–208 °C. ^1H NMR (400 MHz; DMSO- d_6): δ 10.09 (s, 1H), 8.56 (d, $J = 6.1$ Hz, 2H), 8.02–7.96 (m, 1H), 7.72–7.53 (m, 9H), 3.79–3.70 (m, 2H), 2.86–2.76 (m, 2H), 2.53–2.50 (m, 1H), 1.90–1.80 (m, 2H), 1.65–1.53 (m, 2H). ^{13}C NMR (101 MHz, DMSO- d_6): δ 173.3, 150.6, 146.8, 140.7, 136.3, 134.9, 132.7, 131.98, 131.86, 131.81, 131.3, 129.24, 129.13, 128.3, 127.6, 121.0, 119.94, 119.85, 45.2, 42.1, 28.5. ESI-MS ($\text{M}^+ + \text{H}$): 456. HRMS-ESI+: calculated for $\text{C}_{23}\text{H}_{22}\text{ClN}_3\text{O}_3\text{S} + \text{H}$: 456.1149; Found: 456.1129.

1-((2-chlorophenyl)sulfonyl)-N-(4-(6-methylpyridin-2-yl)phenyl)piperidine-4-carboxamide (**4k**) was obtained as a white solid in the amount of 0.028 g, (31 % yield): mp: 129–130 °C. ^1H NMR (400 MHz; DMSO- d_6): δ 10.04 (s, 1H), 8.04–7.97 (m, 3H), 7.74–7.65 (m, 6H), 7.60–7.54 (m, 1H), 7.15–7.13 (m, 1H), 3.78–3.72 (m, 2H), 2.87–2.78 (m, 2H), 2.55–2.52 (m, 1H), 1.89–1.82 (m, 2H), 1.66–1.55 (m, 2H). ^{13}C NMR (101 MHz, DMSO- d_6): δ 173.2, 158.0, 155.3, 140.3, 137.7, 136.3, 134.9, 133.9, 132.8, 132.0, 131.3, 128.3, 127.3, 121.8, 119.5, 117.0, 45.2, 42.1, 28.5, 24.8. ESI-MS ($\text{M}^+ + \text{H}$): 470. HRMS-ESI+: calculated for $\text{C}_{24}\text{H}_{24}\text{ClN}_3\text{O}_3\text{S} + \text{H}$: 470.1305; Found: 470.1289.

1-((2-chlorophenyl)sulfonyl)-N-(4-(4-methylpyridin-2-yl)phenyl)piperidine-4-carboxamide (**4l**) was obtained as a white solid in the amount of 0.068 g, (73 % yield): mp: 129–130 °C. ^1H NMR (400 MHz; DMSO- d_6): δ 10.05 (s, 1H), 8.45 (dd, $J = 5.0$, 0.4 Hz, 1H), 8.02–7.99 (m, 3H), 7.73–7.55 (m, 6H), 7.11 (ddd, $J = 5.0$, 1.5, 0.7 Hz, 1H), 3.78–3.74 (m, 2H), 2.86–2.79 (m, 2H), 2.49 (dt, $J = 3.7$, 1.8 Hz, 3H), 1.88–1.85 (m, 2H), 1.65–1.57 (m, 2H). ^{13}C NMR (101 MHz, DMSO- d_6): δ 173.2, 155.9, 149.6, 148.1, 140.3, 136.3, 134.9, 133.9, 132.8, 132.0, 131.3, 128.3, 127.3, 123.4, 120.7, 119.5, 45.2, 42.1, 28.5, 21.1. ESI-MS ($\text{M}^+ + \text{H}$): 470. HRMS-ESI+: calculated for $\text{C}_{24}\text{H}_{24}\text{ClN}_3\text{O}_3\text{S} + \text{H}$: 470.1305; Found: 470.1284.

1-((2-chlorophenyl)sulfonyl)-N-(4-(5-methylpyridin-3-yl)phenyl)piperidine-4-carboxamide (**4m**) was obtained as a white solid in the amount of 0.037 g, (40 % yield): mp: 126–127 °C. ^1H NMR (400 MHz; DMSO- d_6): δ 10.03 (s, 1H), 8.64 (d, $J = 2.0$ Hz, 1H), 8.35 (d, $J = 1.3$ Hz, 1H), 8.00 (dd, $J = 7.9$, 1.4 Hz, 1H), 7.84 (td, $J = 2.1$, 0.6 Hz, 1H), 7.70–7.61 (m, 6H), 7.59–7.52 (m, 2H), 3.77–3.74 (m, 2H), 2.86–2.79 (m, 2H), 2.33 (s, 3H), 1.88–1.84 (m, 2H), 1.65–1.55 (m, 2H). ^{13}C NMR (101 MHz, DMSO- d_6): δ 173.2, 148.8, 144.9, 139.6, 136.3, 134.9, 134.4, 133.4, 132.7, 132.08, 131.98, 131.87, 131.3, 129.25, 129.13, 128.3, 127.5, 120.0, 45.2, 42.1, 28.5, 18.3. ESI-MS ($\text{M}^+ + \text{H}$): 470. HRMS-ESI+: calculated for $\text{C}_{24}\text{H}_{24}\text{ClN}_3\text{O}_3\text{S} + \text{H}$: 470.1305; Found: 470.1287.

1-((2-chlorophenyl)sulfonyl)-N-(4-(2-methylpyridin-4-yl)phenyl)piperidine-4-carboxamide (**4n**) was obtained as a white solid in the amount of 0.056 g, (60 % yield): mp: 127.5–130 °C. ^1H NMR (400 MHz; DMSO- d_6): δ 10.12 (s, 1H), 8.45–8.42 (m, 1H), 8.02–7.98 (m, 1H), 7.76–7.60 (m, 6H), 7.59–7.53 (m, 2H), 7.44 (dd, $J = 5.3$, 1.5 Hz, 1H), 3.80–3.72 (m, 2H), 2.87–2.76 (m, 2H), 2.54–2.51 (m, 1H), 1.90–1.79 (m, 2H), 1.66–1.49 (m, 2H). ^{13}C NMR (101 MHz, DMSO- d_6): δ 173.3, 158.9, 149.9, 147.1, 140.6, 136.3, 134.9, 133.0, 132.7, 132.15, 131.99, 131.87, 131.3, 129.26, 129.14, 128.3, 127.6, 120.3, 119.9, 118.2, 116.2, 45.2, 42.1, 28.5, 24.6. ESI-MS ($\text{M}^+ + \text{H}$): 470. HRMS-ESI+: calculated for $\text{C}_{24}\text{H}_{24}\text{ClN}_3\text{O}_3\text{S} + \text{H}$: 470.1305; Found: 470.1289.

2.3. Measurement of inhibitor potencies on sEH and FAAH

The IC₅₀ values were determined using FAAH and sEH fluorescent-based inhibition assays as previously described [34,35]. For the FAAH assay, *N*-(6-methoxypyridin-3-yl) octanamide was used as the substrate at a final concentration of 50 μ M. For the sEH assay, cyano (6-methoxynaphthalen-2-yl)methyl((3-phenyloxiran-2-yl)methyl) carbonate was used at a final concentration of 5 μ M. Enzymes were pre-incubated with inhibitors for 5 min in sodium phosphate buffer (0.1 M, pH 8.0, containing 0.1 mg/mL bovine serum albumin for FAAH, and 0.1 M, pH 7.4, containing 0.1 mg/mL bovine serum albumin for sEH) at 37 °C before substrate addition. FAAH activity was measured by detecting the formation of 6-methoxypyridin-3-amine with excitation at 303 nm and emission at 394 nm at 37 °C. sEH activity was measured by detecting the formation of 6-methoxynaphthaldehyde with excitation at 330 nm and emission at 465 nm at 37 °C. All assays were conducted in triplicate. The IC₅₀ value, defined as the concentration of inhibitor required to reduce enzyme activity by 50 %, was calculated using linear regression from at least five data points, ensuring a minimum of two points on either side of the IC₅₀ within the linear region of the curve.

2.4. Solubility assay

Water solubility was determined using turbidity (light scattering) principle. In short, serial 2-fold dilutions of a tested compound in an organic solvent are rapidly diluted 20-fold with sodium phosphate buffer (0.1 M, pH = 7.4), in a 96-well format. The plate is then read for turbidity (light scattering) in a spectrophotometer. The highest concentration of the compound that does not have appreciable turbidity is the solubility of the compound within a factor of 2. Turbidity is measured at 800 nm wavelength.

2.5. Microsomal stability assay in liver microsomes

The test compound was prepared as a 1 mM solution in DMSO, and 1 μ L of this solution was preincubated at 37 °C for 5 min in a mixture consisting of 924 μ L of phosphate buffer (0.1 M, pH 7.4) and 25 μ L of liver microsome mix. Following the 5-min preincubation, the reaction was initiated by adding 50 μ L of an NADPH regenerating system. This system was prepared by dissolving 121 mg of glucose-6-phosphate and 59 mg of NADPH in 2.2 mL of 100 mM PBS buffer, followed by the addition of 800 μ L of glucose 6-phosphate dehydrogenase (100 U/mL) from baker's yeast and 1 mL of 400 mM MgCl₂. The reaction was quenched by adding 450 μ L of methanol at 0, 10, 20, 30, and 60 min. Samples were then centrifuged at 13,500 RPM for 5 min at 4 °C, filtered, and analyzed in SIM mode on LC-MS under isocratic gradient conditions: 20 % eluent A (water + 0.05 % TFA) and 80 % eluent B (acetonitrile + 0.05 % TFA) for 5 min. The peak area response ratio relative to an internal standard was recorded, and the *in vitro* intrinsic clearance was calculated (refer to [Supplementary Data 2](#)), where *k* represents the negative gradient of the natural logarithm of the peak area ratio plotted against time [36].

2.6. Molecular modeling

Docking experiments were conducted using ICM Pro software (Molsoft LLC). A human FAAH homology model was prepared according to a previously published procedure, where the crystal structure of humanized-rat FAAH conjugated with the covalent inhibitor URB597 (PDB: 3LJ7) was used as a template [25]. All inhibitors, including URB597 and TPPU, were docked into this homology model in accordance with the software's guidelines, with the docking thoroughness set to 50. For the human sEH model, the structure was derived from PDB entry 4HAI [37]. The PDB file was converted into an ICM object and optimized using the default program settings. The inhibitor, *N*-cycloheptyl-1-(mesitylsulfonyl) piperidine-4-carboxamide, was manually

removed, and binding pockets were identified prior to conducting the docking experiments.

2.7. Subjects

Given the greater prevalence of trigeminal pain in women versus men [38], female Sprague-Dawley rats purchased from Charles River (Hollister, CA) were used for all *in vivo* experiments. All rats were at least 50 days old by the start of the study. All rats were also randomly assigned to treatment groups. Rats were housed in pairs on a 12/12-h light/dark cycle (lights off at 1100 h). Food and water were available *ad libitum* except during testing procedures. All procedures follow guidelines set forth by ARRIVE and the Guide for the Care and Use of Laboratory Animals and were approved by the California State University, East Bay Institutional Animal Care and Use Committee.

2.7.1. Orofacial formalin test

Rats were briefly anesthetized with isoflurane to improve the accuracy of injection [39]. Dilute formalin (1.5 %, 50 μ L) was injected subcutaneously into the perinasal area lateral to the nose, as this concentration can increase the sensitivity of the model as shown before [40,41]. Rats were placed in Plexiglas chambers on an elevated mesh rack for observation immediately after injection. The time spent exhibiting face-washing behavior, characterized by rubbing the injected area with the ipsilateral fore paw or ipsilateral hind paw was recorded in 3 min intervals for 45 min. Rats were euthanized immediately after data collection.

2.8. Drug treatments

For hyperalgesia experiments, rats were pretreated with an intraperitoneal injection of 10 mg/kg nitroglycerin (NTG; SDM®27, Copperhead Chemical, Tamaqua, PA, USA) using a 26-gauge needle diluted in a propylene glycol:ethanol vehicle 4 h prior to orofacial formalin injection. This dose of nitroglycerin was chosen because it has been shown to enhance orofacial formalin pain in rodents [42].

4f was dissolved in vehicle (20 % DMSO, 20 % cremophor, and 60 % saline) and delivered via intraperitoneal injection. To determine the effects of **4f**, rats received one injection of either vehicle or **4f** (1 or 3 mg/kg). The doses of **4f** were chosen based on our previous work examining the antinociceptive effects of dual sEH/FAAH inhibitors [28]. 30 min after injection, rats were injected with dilute formalin and observed as described above. All experimenters were blinded to drug treatment conditions. All drugs were made immediately before injection.

2.9. Wheel running

Animals were housed in standard rat cages containing metal running wheels with a 33 cm diameter (Starr Life Sciences, Oakmont, PA, USA). The running wheels were counted via VitalView® Activity software to count the number of wheel revolutions. The number of wheel revolutions were collected every 5 min. Rats were allowed to habituate to the running wheel cages for 3 days before data collection. The number of wheel revolutions that occurred over the 23-h period on the third day was used as the baseline measure [43]. Experimental manipulations began the day after baseline assessment. On this day, rats were removed from their cages and weighed. Animals were injected with nitroglycerin (10 mg/kg) and returned to their home cages at the start of the dark cycle (1100 h). All following procedures were conducted under red light to maintain darkness in the room and not disrupt home cage behavior. After 3.5 h, animals then received 3 mg/kg **4f** or vehicle 30 min before orofacial formalin injection and returned to their cages. Finally, animals received an orofacial injection of formalin under light isoflurane anesthesia and returned to their home cages to run. Measurement of wheel running began 2 min after formalin injection to ensure that anesthesia

did not affect running levels. Wheel running data were collected for 1 h following formalin injection. No experimenters were in the room as wheel running data were collected.

2.10. Data analysis

All data are expressed as mean \pm SEM except where stated. Face-washing behavior produced by formalin was analyzed using a *t*-test or one-way analysis of variance (ANOVA) on GraphPad Prism. For wheel running data, an average hourly nighttime running rate on Day 3 was used as the baseline for hourly analysis. All wheel running data are presented as a percent change from each rat's baseline value. Statistical significance was defined as a probability of <0.05 .

3. Results and discussion

3.1. Structure-activity relationship studies

We have previously identified a central pharmacophore required for the dual FAAH/sEH inhibitory activity: a piperidine ring connected via sulfonamide bond to the phenyl ring on the right side, and to the phenyl ring via an amide bond on the left side (Fig. 1) [25]. Our initial SAR study showed that only a halogen group in the ortho position is preferred [28], so we turned our attention to the left side of the pharmacophore, where we tested different bulky hydrophobic moieties [26,27,29,44] and were able to discover several potent dual inhibitors. In addition, the literature review showed that both quinolyl- and pyridyl-moieties attached to piperidine or piperazine rings are present in many potent FAAH inhibitors reported by Cravatt et al., including PF-750 and PF-3845 [45]. Another potent quinolyl-based FAAH inhibitor has been also reported by Wang et al. with IC_{50} value of 21 nM in rat FAAH [46]. Similarly, both groups were present in urea-based sEH inhibitors reported by Kodani et al. [47], and quinolyl-based dual sEH/FAAH inhibitors were explored in our previous work [44]. Encouraged with these findings, we decided to further explore the effects of pyridine ring on the sEH and FAAH inhibition, and the isoquinoline ring, which is structurally very similar to quinoline, but not present in any published sEH or FAAH inhibitors. Our previous biological evaluations showed that benzothiazole and 4-phenylthiazole inhibitors are active in human FAAH, human and rat sEH, but are not active in mouse sEH, and possess low solubility and a rapid intrinsic clearance in liver microsomal liver assays. On the other hand, quinolyl-analogs showed moderate solubility and better stability, i.e. a longer half-life time in plasma stability assay, and were active in all tested species, including mouse sEH, thus in this study we will explore the left side of the pharmacophore by synthesizing the additional two libraries, isoquinolyl- and pyridinyl-, test their effects on the dual FAAH/sEH inhibition and evaluate their several other pharmacokinetic properties. All analogs were synthesized using previously published 4-step reaction procedure [24]. Starting with two

commercially available starting materials, 2-chlorobenzenesulfonyl chloride and methyl 4-piperidinecarboxylate, we were able to obtain the amide **1** using microwave irradiation (Scheme 1) in the moderate yields. The methyl ester group was hydrolyzed using lithium hydroxide and the carboxylic acid **2** was obtained in high yields. In the next step, we coupled the carboxylic acid **2** with the commercially available 4-aminophenylboronic acid, pinacol ester, using EDC-coupling microwave-assisted reaction to get the key intermediate **3**. Finally, we performed a direct coupling of **3** with various bromo-isoquinolines or bromo-pyridines using the Suzuki-Miyaura reaction, and microwave irradiation for 60 min at 110 °C, tetrahydrofuran/water (4:1) mixture as a solvent, potassium carbonate as a base and palladium-tetrakis (triphenylphosphine) as a catalyst. The target analogs **4a-n** were obtained in moderate to high yields, 17–83 %.

Our SAR study starts with Library 1, i.e. the isoquinolyl-analogs **4a-g** (Table 1). We observed that the orientation of the isoquinoline ring does not affect the FAAH inhibition significantly. Analogs **4a** (1-isoquinolyl), **4b** (2-isoquinolynil) and **4f** (7-isoquinolynil) showed very strong FAAH activity, comparable to the previously identified quinolyl-based lead compound JA-112. The other isoquinolyl analogs (**4c**, **4d**, **4e** and **4g**) showed slightly lower activity in FAAH. Again, we observed the species differences in sEH inhibition assays, and most of the isoquinoline analogs were weakly to moderately active in mouse sEH, with **4c** being the most active with the IC_{50} value of 22.3 nM. However, this set of compounds performed much better than the previously reported benzothiazole or 4-phenylthiazole analogs in the mouse sEH inhibition assay, thus we concluded that most of the unfavorable interactions with the mouse sEH binding pocket and dual inhibitors are due to these particular moieties located on the left side of the molecules and not the whole structure. All isoquinoline analogs showed very strong potencies in both rat and human sEH, with compound **4c**, being one of the most potent dual inhibitors identified in this study, with IC_{50} values of 0.4 nM and 0.8 nM in human and rat sEH respectively. Library 2, the pyridinyl-based dual inhibitors, surprisingly showed significant lower activity in the FAAH inhibition assay compared to the compounds from Library 1. This trend was observed in all 7 compounds; however, we were able to establish some SAR conclusions, i.e. the position of the methyl group and nitrogen atom are important for FAAH activity, with **4n** being the most active (IC_{50} = 158.5 nM) and **4l** being the least active with IC_{50} value of 1800 nM. Activity of Library 2 in sEH enzymatic assays followed the similar trends as we observed with Library 1, i.e. compounds were very potent in rat and human sEH and significantly less active in mouse sEH. Compounds **4i** and **4m** were in particular very active, with IC_{50} values in low nanomolar range for both human and rat sEH. We concluded that sEH binding pocket is more flexible and can fit various heterocycles, while in order to achieve a good FAAH activity, the design will need to include at least two aromatic (hetero) rings. Although the Library 2, did not yield any strong dual FAAH/sEH inhibitor, we were still able to establish the SAR and to identify several novel and potent sEH inhibitors, which will be a great addition to the sEH field, especially since sEH inhibitors have been individually investigated as potential therapeutics for pain, inflammatory and neurodegenerative diseases [7,48]. Additionally, Library 2 compounds have a moderate FAAH activity, which might be interesting to explore further, due to the known FAAH/sEH synergism.

Since Library 1, the isoquinolyl-analogs, was active on both FAAH and sEH, we decided to scale up analog **4f** and further test it in rat and human microsomal liver stability assays and in tests of orofacial pain and hyperalgesia in female rats.

3.1.1. Solubility and microsomal liver stability assays

Both metabolic stability and solubility are important drug properties for *in vivo* potency; thus, we determined the water solubility for all newly synthesized analogs in this study (Table 1) and the half-life of the lead compound **4f** in the human and rat hepatic microsomes (Table 2). In general, compounds with less than 31 μ M water solubility are

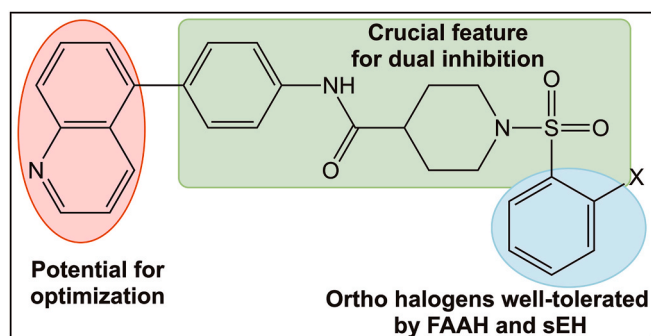
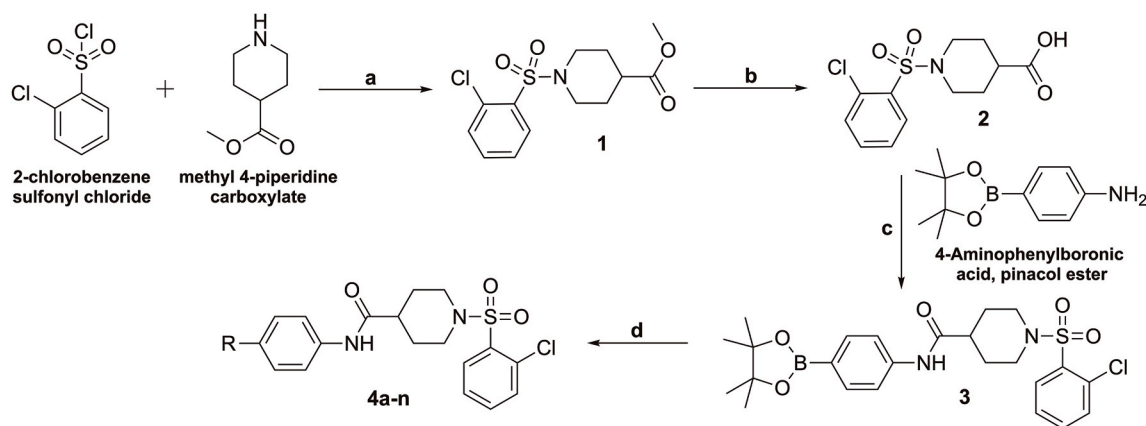


Fig. 1. Summary of previously performed SAR studies (blue), identified pharmacophore for dual FAAH/sEH inhibition (green) and strategy for optimization (red).



Scheme 1. Reagents and conditions: (a) Et₃N, CH₂Cl₂, 20 min, 80 °C, microwave irradiation, 85 %; (b) 4.6 M aq LiOH; THF/H₂O, 16 h, rt, 40 %; (c) EDC, DMAP, CH₂Cl₂, 20 min, 80 °C, microwave irradiation, 68 %; (d) R-Br (see Table 1 for R), Pd(PPh₃)₄; K₂CO₃, THF/H₂O, 60 min, 110 °C, microwave irradiation, 17–83 %.

considered to be poor drug candidates for the *in vivo* studies [49]. Both, the isoquinolinyl- and pyridinyl-analogs showed moderate solubility but isoquinolinyl-compounds possess higher potencies, thus we decided to select these compounds to study further.

We also performed an additional assay to assess the stability of the most potent analog identified in this study, **4f**, in the liver microsomes. Microsomal liver assay (MLA) is a good predictor of a drug liver stability, which is important for the drugs administrated orally due to the first-pass effect. Since one of our goals is to develop an oral analgesic, we decided to test the dual sEH/FAAH inhibitor **4f** in both rat and human liver microsomes as the part of our pre-clinical drug discovery process.

The results are summarized in Table 2, where the stability of **4f** were assessed using apparent intrinsic clearance (CL_{int}) and half-life (t_{1/2}) in rat and human MLA. We noticed a significant species differences, with a moderate half-life in rat MLA of 25.6 min, and a 2-fold better half-life of 58 min in human microsomal assay. We observed moderate clearance rate in both rat and human liver microsomes, with the CL_{int} value of 54 μL/min/mg and 23.7 μL/min/mg, respectively, since the intrinsic clearance values in microsomal assay below 13.2 μL/min/mg are considered as a low clearance and CL_{int} values above 71.9 μL/min/mg are classified as high clearance compounds [36]. We concluded that isoquinoline moiety is showing much better stability in liver microsomes compared to 4-phenylthiazole and benzothiazole (which we reported before) and **4f** represents a viable candidate for the future *in vivo* evaluation, both orally and systemic injection.

3.1.2. Receptor binding

To determine whether **4f** binds to opioid or serotonin (5-HT) receptors, the Psychoactive Drug Screening Program (PDSP) provided by the National Institutes of Mental Health (NIMH) evaluated **4f** against a variety of receptor subtypes presented in the Table 3 below [50]. Opioid receptors were chosen given their obvious role in pain relief. Although there are seven subtypes of serotonin receptors, the three subtypes that are most relevant to migraine pathophysiology (5-HT₁, 5-HT₂, and 5-HT₃) were chosen to determine potential anti-migraine actions of **4f** [51]. Several values for various receptors including the kappa opioid receptor and 5-HT_{1B/1D/2A/2C} receptors were non-null indicating that there may be activity of **4f** at these receptors. However, the minimum threshold of 50 % inhibition was not reached for any receptor [50] likely indicating no significant binding at these receptors and were therefore not tagged for secondary binding assays.

3.1.3. Molecular modeling

To better understand the binding modes of **4f** in binding pockets of FAAH and sEH, we decided to use the molecular modeling studies and docking experiments. FAAH is known for its unusual catalytic triad, S241–S217–K142, responsible for the hydrolysis of the substrate. The X-

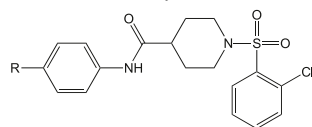
ray crystal structure of the human FAAH is not available, but there are several rat FAAH crystal structures reported with the good resolution. We decided to use PDB: 3LJ7, a 3D-crystal structure of humanized-rat FAAH conjugated with the covalent inhibitor URB597, which has been reported at 2.3 Å [52]. Using this structure as a template, we first built a human homology model of FAAH and validated it using several known platforms [53], available at UCLA-DOE lab server. Next, we performed the docking experiments using ICM Pro molecular modeling software [54] and obtained the results shown in Fig. 2A and B.

The docking pose of **4f** analog in FAAH homology model revealed that it binds to the proximity of the catalytic triad, i.e. the amide bond of **4f** forms a hydrogen bond with S241 (distance 2.79 Å) and in addition the phenyl ring next to the amide bond is engaged in hydrophobic interaction with S217. There are several non-covalent interactions of 2-chlorophenyl moiety with the surrounding amino acid residues, L404, M495, T488, F432, F381, L380 and V491, which all contribute to the stabilization of **4f** in the FAAH binding pocket. Next, we noticed many non-covalent interactions of the isoquinolinyl moiety and several amino acid residues, Y271, L278, G268, M191, L266, K267, C269 and V270. We also observed that isoquinoline ring is orientated to the solvent open space, which we hypothesize is the reason why this binding pocket can fit differently orientated isoquinolinyl-moieties as well as many various bulky hydrophobic groups, such as benzothiazoles, 4-phenylthiazoles and quinolines. We believe that the nitrogen position within isoquinoline ring does not play an important role in binding, but it is an important contributor for the overall inhibitory potency through the shape and polarity. Indeed, the biological evaluations (Table 1) confirm this theory since all isoquinoline analogs, **4a-g** have similar activity in FAAH. On the other hand, pyridyl-analogs, **4h-n**, showed significantly diminished FAAH activity compared to isoquinoline derivatives in the *in vitro* inhibitory assays, suggesting that although this part is not directly engaged in the binding with the enzyme, the bulkiness of two fused aromatic rings is necessary for the optimized binding. All important contacts of **4f** with the FAAH binding sites and their distances are listed in Table S1.

Docking experiments in sEH were more direct, since there are many X-ray crystallographic structures of human sEH with inhibitors available at high resolution. We decided to use PDB: 4HAI, which contains the amide-piperidine inhibitor discovered in our lab previously [37]. The catalytic triad of sEH is composed of D335-Y383-Y466, and we observed that **4f** binds in the catalytic site near these three key amino acid residues, Fig. 3A and B. The amide bond of **4f** is forming the hydrogen bond with Y466 (the oxygen atom is acting as a hydrogen bond acceptor, with the distance of 2.65 Å) and there are several noncovalent interactions that are important for the binding of this analog in the sEH binding site. The 2-chloro moiety is engaged in the hydrophobic interactions with M419, W525, L417, L408 and L428. The piperidine ring is stabilized

Table 1

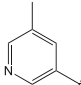
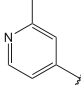
Fatty acid amide hydrolase (FAAH) and soluble epoxide hydrolase (sEH) inhibitory activities.



Compound	R	Human FAAH IC ₅₀ (nM) ^a	Human sEH IC ₅₀ (nM) ^a	Mouse sEH IC ₅₀ (nM) ^a	Rat sEH IC ₅₀ (nM) ^a	Solubility (μM) ^b
URB597	—	35	—	—	—	—
t-TUCB	—	—	0.3	1.6	9.1	—
SP 4-5		7.0	9.6	812.8	3.9	12.85
JA-112		19.6	1.7	17.2	2.0	30.85
4a		25.8	3.7	282.9	3.7	55.95
4b		5.0	18.7	235.8	11.5	51.65
4c		64.6	0.4	22.3	0.8	49.17
4d		62.5	0.4	30.6	2.2	40.04
4e		55.9	1.8	51.3	0.5	55.82
4f		15.5	2.2	106.9	1.0	54.37
4g		43.6	1.4	69.0	4.7	65.58
4h		263.3	1.7	188.3	1.9	66.67
4i		551.6	1.3	126.6	2.8	51.08
4j		198.1	1.8	133.2	3.1	50.85
4k		291.3	4.7	225.9	1.6	43.39
4l		1800.1	5.1	498.9	10.3	36.36

(continued on next page)

Table 1 (continued)

Compound	R	Human FAAH IC50 (nM) ^a	Human sEH IC50 (nM) ^a	Mouse sEH IC50 (nM) ^a	Rat sEH IC50 (nM) ^a	Solubility (μM) ^b
4m		209.0	2.6	175.3	1.1	49.35
4n		158.5	5.8	258.8	3.6	53.03

^a Reported IC50 values are the average of three replicates. The assay as performed here has a standard error between 10 and 20 % suggesting that differences of two-fold or greater are significant.

^b Assay done in 0.1 M sodium phosphate buffer pH = 7.4, at 24 °C.

Table 2

Stability in rat and human Liver Microsomes Assay (MLA) for 4f.

MLA	t1/2 (min) ^a	CL _{int,app} (μL/min/mg) ^b
Rat	25.6	54
Human	58	23.7

^a Data represent averages of duplicate or triplicate determination. LMT1/2 is the half-life in rat or human liver microsomes.

^b Apparent intrinsic clearance (CL_{int,app}) was calculated based on CL_{int} = k/P, where k is the elimination rate constant and P is the protein concentration in the incubation.

Table 3

NIMH PDSP screening results for binding of 4f to opioid and serotonin receptor subtypes.

Receptor	Inhibition (%) ^a	P _(value = 0) ^b
Delta opioid (DOR)	3.10 ± 1.53	0.1358
Kappa opioid (KOR)	−18.12 ± 2.56	0.0058 ^c
Mu opioid (MOR)	10.62 ± 4.75	0.1114
5-HT _{1A}	4.83 ± 2.43	0.1410
5-HT _{1B}	12.45 ± 2.29	0.0122 ^c
5-HT _{1D}	40.9 ± 11.15	0.0350 ^c
5-HT _{2A}	17.38 ± 4.69	0.0341 ^c
5-HT _{2C}	21.47 ± 4.63	0.0189 ^c
5-HT ₃	−0.28 ± 5.94	0.9654

^a Data represent average ± SEM of inhibition (n = 4) for 4f tested at 10 μM.

^b Probability that results are equal to zero (no inhibition nor activation of the receptor).

^c Significantly not null at p < 0.05.

with F387, Y383, F267 and D335. Next, we observed the interactions of isoquinolinyl ring and W336, N472, M469, M339, I375, F381 and P371 amino acid residues.

Again, we noticed that this part of the molecule is orientated towards the solvent, which we believe is the reason why this part of the molecule is particularly good for the further optimization. Here, we again hypothesized that the nitrogen atom does not contribute to the binding significantly, which is supported with the low nanomolar potencies in human sEH for all analogs from this series, **4a-g**, but it is important for the activity by providing the overall 3D shape and polarity. The pyridyl-analogs, **4h-n**, were also very potent in the biological assays, providing more information of the human sEH and it further supports the theory that this part of the molecule is not engaged in the significant binding interactions within the binding pocket. The list of the contacts and distances of **4f** with the sEH binding site are listed in Table S2.

3.1.4. In vivo assessment

To model orofacial hyperalgesia in rats, we adapted the orofacial formalin test and used nitroglycerin to sensitize animals. Nitroglycerin is an organic nitrate that has frequently been used to mimic migraine-like

symptoms in animal models of migraine and evaluate potential therapies for trigeminal pain disorders [55]. Nitroglycerin exerts its actions by serving as a nitric oxide donor and a vasodilator in the nervous system. Nitroglycerin has been demonstrated to enhance peripheral pain [56], enhance trigeminal pain and produce trigeminal hyperalgesia [21, 42,57], and directly activate migraine-relevant pain structures in humans and rats [55], indicating that it interacts directly with headache-specific structures and mechanisms. Given this, we used nitroglycerin to enhance pain produced by orofacial formalin to evaluate orofacial hyperalgesia.

The enhancement of orofacial pain is likely due to a hypersensitivity to noxious orofacial stimuli due to nitroglycerin producing central sensitization [58]. These same mechanisms may be responsible for mediating certain clinical features of headache and trigeminal pain in humans such as throbbing headache or cranial hypersensitivity [58]. One unique feature of nitroglycerin is its ability to produce hyperalgesia well after the injection, on the order of 2–4 h in most animal studies [58]. The reason for this is likely because nitroglycerin-induced activation of trigeminal neurons peaks at 3–4 h following injection [58,59]. Therefore, the use of this model helps better understand the neural and orofacial components of headache and trigeminal pain and can be effectively used to screen potential therapies. We used this model further to evaluate the antinociceptive effects of **4f** against orofacial hyperalgesia.

Fig. 4 shows the time spent rubbing the injected area over the 45 min period following orofacial injection of formalin, which is 30 min after injection of **4f** or vehicle, and 240 min after injection of nitroglycerin. A one-way analysis of variance revealed that pain behaviors in female rats treated with **4f** was significantly different from rats treated with vehicle [F (2, 23) = 6.92, p = 0.005]. A Tukey post-hoc test revealed that rats treated with the high dose of **4f** (3 mg/kg) rubbed the injected area for significantly less time than vehicle-treated rats (p = 0.004) and rats treated with the low dose of **4f** (1 mg/kg; p = 0.04). There were no significant differences in the time spent rubbing between vehicle- and 1 mg/kg **4f**-treated rats (p = 0.58).

These results indicate that dual FAAH/sEH inhibition produced by a high, but not low, dose of **4f** can alleviate orofacial hyperalgesia produced by a pretreatment of nitroglycerin in rats (Fig. 4). Our previous work has demonstrated antinociceptive properties of dual FAAH/sEH inhibitors as low as 1 mg/kg for other types of formalin-induced pain [24,26]; thus, the type of pain (orofacial vs. peripheral) may drive these differences.

Other studies have demonstrated similar anti-hyperalgesic effects with peripherally-restricted FAAH inhibitors such as URB937 [57]. Greco et al. demonstrated that 1 mg/kg of this inhibitor reversed NTG-induced trigeminal hyperalgesia in rats, and that this reversal was dependent on activation of the CB₁ receptor [57]. These effects can likely be explained by the increased tone of lipid mediators including endocannabinoids following inhibition of FAAH in several areas of the nervous system that are responsible for trigeminal pain such as the

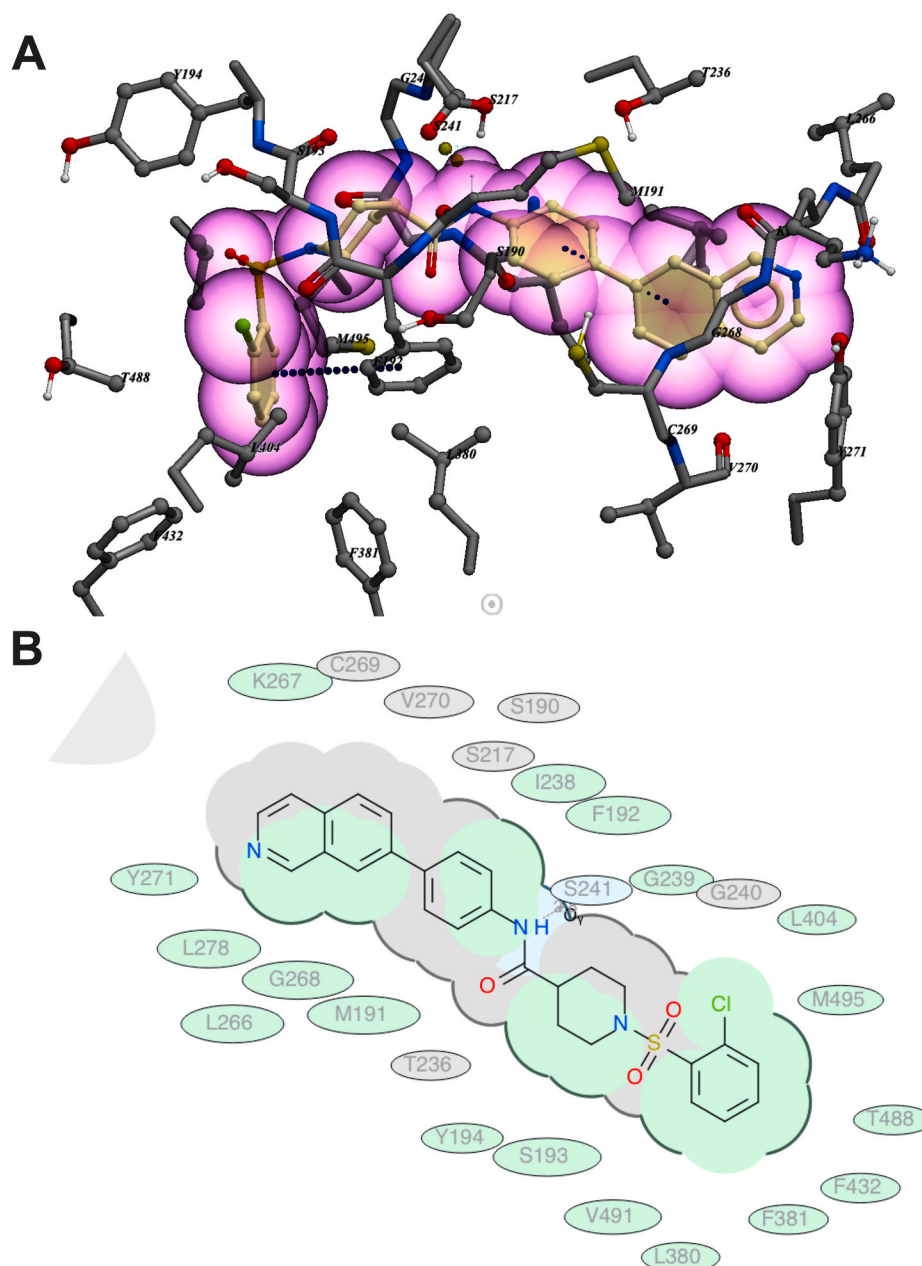


Fig. 2. A) 3D docking pose of the inhibitor **4f** in the binding site of FAAH. B) 2D representation of **4f** in the binding site of FAAH. The green and gray amino acid residues represent nonpolar and hydrophobic contacts, while blue represents hydrogen bonding with the ligand **4f**.

trigeminal ganglion [57]. Although we did not directly measure endocannabinoid levels following **4f** administration, we hypothesize that activation of peripheral CB₁ receptors may also contribute to the antinociception produced by **4f** in Fig. 4.

Given the pharmacology of **4f** and the synergy between sole FAAH and sole sEH inhibitors [23], the effects of FAAH may be compounded by the effects of sEH on orofacial hyperalgesia. Previous studies have shown that inhibition of sEH can alleviate pain associated with inflammation of orofacial regions such as the temporomandibular joint [19,60]. Studies have shown that local administration of the sEH inhibitor, TPPU, prevented formalin-induced hyperalgesia within the temporomandibular joint (TMJ) [61]. More importantly, this effect was due to the inhibition of mast cell degranulation within the TMJ [61]. Nitroglycerin has also been shown to degranulate mast cells in regions of the nervous system that are responsible for producing trigeminal pain such as the dura mater two to 6 h after NTG administration [62]. We had

pre-treated rats with nitroglycerin for 4 h prior to **4f** administration; therefore, it may be possible that the sEH component of the actions of **4f** are non-neuronal and are simply due to the inhibition of mast cell degranulation in the peripheral nervous system.

A combination of both FAAH and sEH mechanisms (e.g., CB₁ receptor activation and inhibition of NTG-induced mast cell degranulation) may explain the anti-hyperalgesic properties of **4f**. These studies provide an initial proof-of-concept that dual FAAH/sEH inhibition can reverse orofacial hyperalgesia in the rat.

Given the anti-hyperalgesic effects of 3 mg/kg **4f** in Fig. 4, we wanted to determine whether this same dose was efficacious against orofacial pain in non-hyperalgesic rats. That is, these rats were not pre-treated with nitroglycerin. Fig. 5A shows the amount of time spent rubbing the injected area following formalin injection. There was no significant difference between vehicle or **4f**-treated animals [$t(11) = 0.09$, $p = 0.93$]. Consistent with our findings with other dual FAAH/sEH

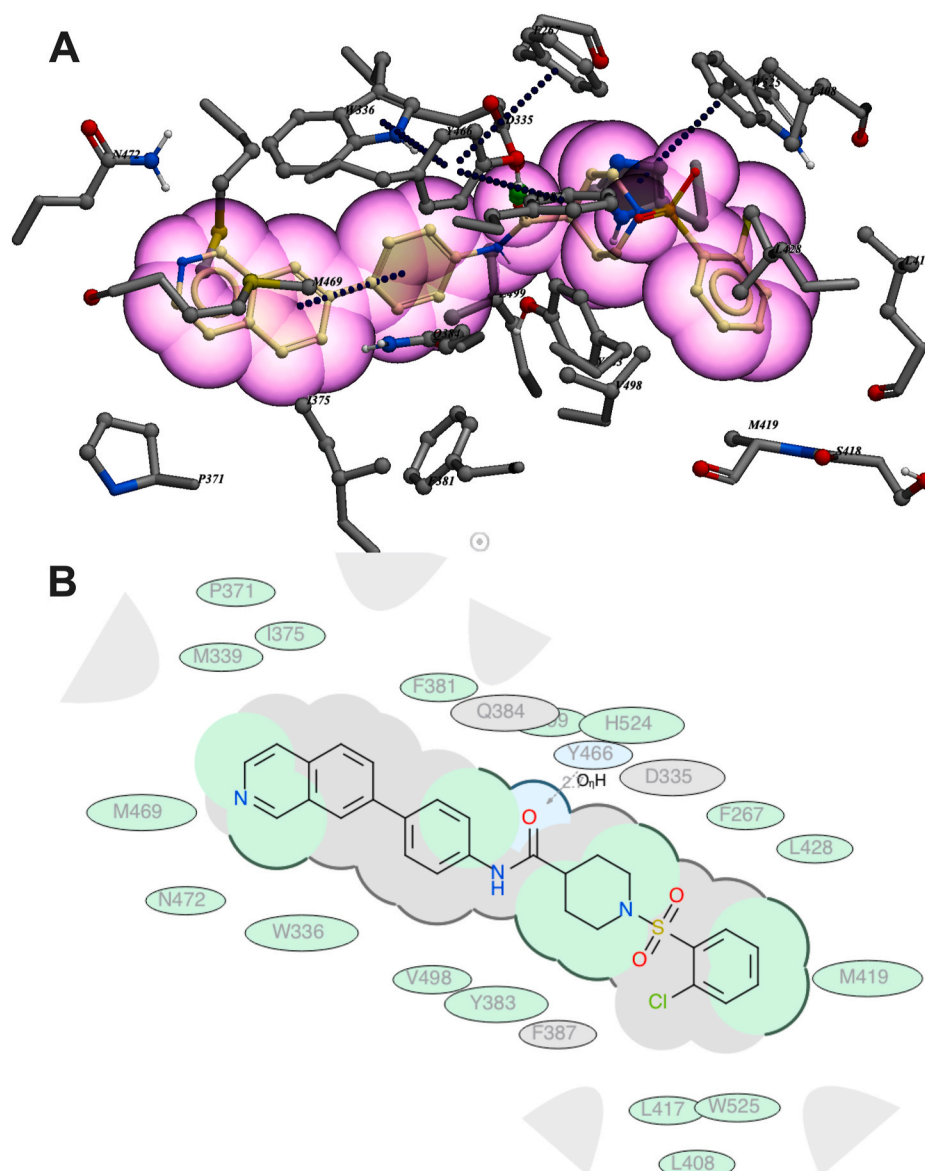


Fig. 3. A) 3D docking pose of the inhibitor 4f in the binding site of sEH. B) 2D representation of 4f in the binding site of sEH. The green and gray amino acid residues represent nonpolar and hydrophobic contacts, while blue represents hydrogen bonding with the ligand 4f.

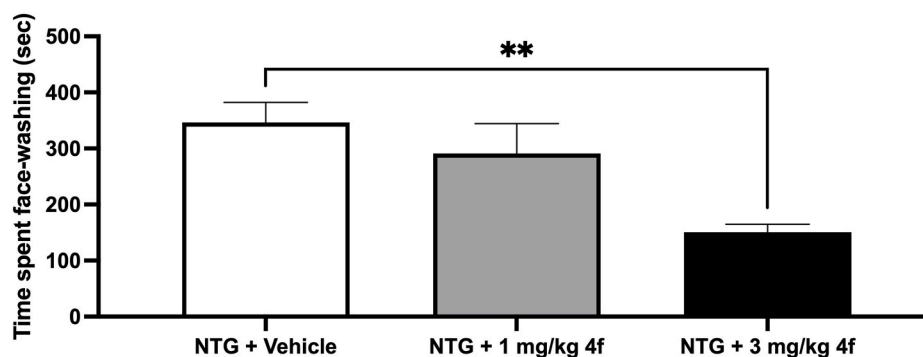


Fig. 4. Antinociceptive effects of 4f on orofacial hyperalgesia using the orofacial formalin test. The time spent rubbing the injected area over the 45 min observation period following injection is represented. NTG = 10 mg/kg nitroglycerin. ** indicates $p < 0.01$. $n = 8-9$ /group.

inhibitors [29], this indicates that 4f may not have an acute antinociceptive effect against formalin-induced inflammatory pain in the orofacial region.

The mechanisms explaining this lack of effect could be due to the differing effects that FAAH and sEH inhibition have on the release of calcitonin gene-related peptide (CGRP), a pro-nociceptive peptide

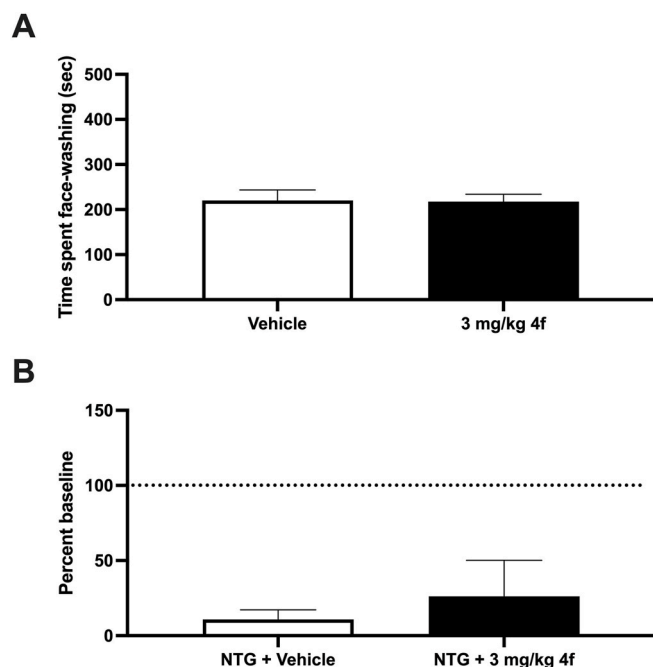


Fig. 5. Effects of 4f on formalin-induced orofacial inflammatory pain and pain-depressed wheel running. A) Animals were treated 30 min before orofacial formalin injection with either vehicle or 3 mg/kg 4f. The time spent rubbing the injected area following injection is represented. B) Baseline levels of running were obtained the night before the injections and represented as 100 % (dotted line). Animals were then pre-treated with NTG 4 h before formalin injection and either vehicle or 3 mg/kg 4f 30 min before formalin injection. The amount of wheel running as a percent of the rat's baseline running levels is presented. $n = 6-7/\text{group}$.

important for trigeminal pain processing. Studies have shown that sole inhibition of FAAH decreases the level of CGRP following administration of formalin in various regions of the peripheral and central nervous systems [63]. A decrease in CGRP likely explains any antinociceptive effect. However, other studies have shown that inhibition of sEH can sensitize the release of CGRP to enhance pain processing [64]. Moreover, other studies have shown that pretreating mice with a sole sEH inhibitor does not decrease CGRP levels in trigeminal neurons [65]. Taken together, it may be possible that a balance between the sensitization and inhibition of CGRP release could explain the lack of an antinociceptive effect of 4f. This balance may be disrupted in states of hyperalgesia or after nitroglycerin administration, which may explain the antinociceptive effects seen under states of hyperalgesia and not acute pain. Other studies have also demonstrated similar effects where inhibition of FAAH alone or FAAH and monoacylglycerol lipase (MAGL) produces pain relief under states of hyperalgesia, but not acute pain [57, 63]. Future work will evaluate this balance to understand the effects of dual FAAH/sEH inhibition on states of hyperalgesia vs. acute pain. Additional studies such as pharmacokinetics (tissue distribution, bioavailability, C_{max} , or AUC) or testing 4f in the presence of sole FAAH/sEH drugs will also reveal the potential sites and mechanisms of action of 4f.

We also evaluated the efficacious dose of 4f in a test of pain-depressed home cage wheel running, a measure of the functional component of pain. Pain decreases activity in rats, just like it does in humans. Therefore, a good therapy should not only eliminate pain, but it should also restore normal activity [31]. Although pain decreased baseline levels of running in both groups, there was no significant difference between vehicle or 4f-treated animals [$t(10) = 0.62$, $p = 0.55$]. A lack of restoration of wheel running could be due to several variables. While this likely indicates a lack of efficacy against the functional component of orofacial hyperalgesia, it may also be due to adverse

locomotor effects associated with higher doses of dual FAAH/sEH inhibitors when administered during hyperalgesic states. Our previous work demonstrated that 3 mg/kg of a dual FAAH/sEH inhibitor does not depress wheel running in the absence of pain [28]; therefore, higher doses of 4f may be needed to reverse the functional component of orofacial hyperalgesia. Interestingly, this finding is also consistent with other findings indicating that inhibition of FAAH and MAGL only decrease NTG-induced hyperalgesia and not the other functional components of migraine-associated pain in rats [63]. Nonetheless, these studies are consistent with other findings that trigeminal pain depresses running in rats [66–68] and the present data are the first to demonstrate decreased home cage wheel running following orofacial hyperalgesia in rats.

4. Conclusion

Our SAR study revealed that the isoquinoline ring is well tolerated in both FAAH and sEH binding sites, yielding inhibitors with the IC_{50} values in the nanomolar range, suggesting that the enhanced potencies of this library is due to increased polarity and basicity rather than the orientation of the isoquinoline moiety. In addition, our SAR shows that the isoquinolinyl-group is moderately active in mouse sEH, compared to 4-phenylthiazole and benzothiazole dual inhibitors that were not active in mouse sEH inhibition assays. The introduction of the pyridine ring yielded very potent sEH inhibitors but showed that FAAH binding pocket prefers more bulkier hydrophobic groups (e.g. two aromatic rings) which led to only moderate potencies of the pyridyl-group analogs in the FAAH inhibition assays. The pyridyl-analogs showed moderate solubility, and possess strong sEH inhibition potencies, thus these inhibitors might be good lead compounds to study in other medicinal chemistry settings. We also observed, in general, higher solubility of isoquinolinyl analogs compared to benzothiazole and quinolinyl analog, SP 4–5 and JA-112 respectively, however, solubility of dual inhibitors is something that should be improved in the future follow-up studies, by introducing more nitrogen atoms and/or polar groups. The most active dual inhibitor discovered in this study, 4f, was evaluated in microsomal liver stability assay and we noticed a significant species differences, i.e. this analog exhibited a moderate half-life of 25.6 min and 58 min in rat and human liver microsomes, respectively. Primary binding studies demonstrated that 4f produces its effects via non-opioid and non-serotonergic mechanisms. Intraperitoneal administration of 4f in rats pre-treated with nitroglycerin, to model orofacial hyperalgesia, produced dose-dependent antinociceptive effects. The high dose of 4f was effective at reducing pain behaviors in hyperalgesic rats; however, this same dose was ineffective at alleviating orofacial inflammatory pain and restoring pain-depressed wheel running. Our findings indicate that dual inhibition of FAAH and sEH using 4f may inhibit the sensory, but not functional, component of orofacial hyperalgesia. Future studies will evaluate the contribution of both enzymes in these antinociceptive effects to better design treatments for trigeminal pain disorders.

CRedit authorship contribution statement

Daniel Carr: Writing – original draft, Methodology, Investigation. **Siena Gunari:** Writing – original draft, Methodology, Investigation. **Gabrielle Gorostiza:** Methodology, Investigation. **Madison Mercado:** Methodology, Investigation. **Lucy Pavana:** Methodology, Investigation. **Leah Duong:** Methodology, Investigation. **Karen Gomez:** Methodology, Investigation. **Steve Salinas:** Methodology, Investigation. **Coral Garcia:** Methodology, Investigation. **Amanda Tsang:** Methodology, Investigation. **Christophe Morisseau:** Writing – review & editing, Resources, Investigation. **Bruce D. Hammock:** Writing – review & editing, Resources, Investigation. **Stevan Pecic:** Writing – original draft, Supervision, Methodology, Investigation, Conceptualization. **Ram Kandasamy:** Writing – original draft, Methodology, Investigation, Conceptualization.

Declaration of competing interest

The authors declare that they have no known competing financial interests or personal relationships that could have appeared to influence the work reported in this paper.

Acknowledgments

This work was supported by the National Institute of General Medical Sciences of the National Institutes of Health under Award Number R16 GM150781. No authors declare a conflict of interest. Partial support was provided by NIH-NIEHS (RIVER Award) R35 ES030443, NIH-NINDS U54 NS127758 (Counter Act Program), NIH-NIGMS R16GM149204, and NIH-NIEHS (Superfund Award) P42 ES004699. Instrumentation support was provided by the National Institutes of Health under award number R16 GM149204-02S1 for acquisition of an LC-MS. SS was supported by Project RAISE, U.S. Department of Education HSI-STEM award P031C160152 and Project RAISER U.S. Department of Education HSI-STEM award P031C210118. Binding data was generously provided by the National Institute of Mental Health's Psychoactive Drug Screening Program, Contract # 75N95023C00021 (NIMH PDSP). The NIMH PDSP is Directed by Bryan L. Roth MD, PhD at the University of North Carolina at Chapel Hill and Project Officer Jamie Driscoll at NIMH, Bethesda MD, USA. The authors would like to express their gratitude to Alton Lo for his invaluable assistance with the data analysis and Jennifer Novoa for her technical assistance with the animal studies. We thank Dr. Paula Hudson (CSUF) for obtaining the HRMS data - instrumentation support was provided by the National Science Foundation MRI (CHE1726903) for acquisition of an UPLC-MS.

Appendix A. Supplementary data

Supplementary data to this article can be found online at <https://doi.org/10.1016/j.bbrep.2025.102009>.

Data availability

Data will be made available on request.

References

- [1] M.A. Moskowitz, The neurobiology of vascular head pain, *Ann. Neurol.* 16 (2) (1984) 157–168.
- [2] C. Bernstein, R. Burstein, Sensitization of the trigeminovascular pathway: perspective and implications to migraine pathophysiology, *J. Clin. Neurol.* 8 (2) (2012) 89–99.
- [3] H.K. Kim, et al., The trigeminal sensory system and orofacial pain, *Int. J. Mol. Sci.* 25 (20) (2024).
- [4] C. Cameron, et al., Triptans in the acute treatment of migraine: a systematic review and network meta-analysis, *Headache* 55 (Suppl 4) (2015) 221–235.
- [5] M. De Felice, et al., Triptan-induced latent sensitization: a possible basis for medication overuse headache, *Ann. Neurol.* 67 (3) (2010) 325–337.
- [6] F. Antonaci, et al., Recent advances in migraine therapy, *SpringerPlus* 5 (2016) 637.
- [7] K.M. Wagner, et al., Soluble epoxide hydrolase as a therapeutic target for pain, inflammatory and neurodegenerative diseases, *Pharmacol. Ther.* 180 (2017) 62–76.
- [8] J.E. Schlosburg, S.G. Kinsey, A.H. Lichtman, Targeting fatty acid amide hydrolase (FAAH) to treat pain and inflammation, *AAPS J.* 11 (1) (2009) 39–44.
- [9] J.W. Newman, C. Morisseau, B.D. Hammock, Epoxide hydrolases: their roles and interactions with lipid metabolism, *Prog. Lipid Res.* 44 (1) (2005) 1–51.
- [10] C. Morisseau, B.D. Hammock, Impact of soluble epoxide hydrolase and epoxyeicosanoids on human health, *Annu. Rev. Pharmacol. Toxicol.* 53 (2013) 37–58.
- [11] K.M. Wagner, J. Atone, B.D. Hammock, Soluble epoxide hydrolase inhibitor mediated analgesia lacks tolerance in rat models, *Brain Res.* 1728 (2020) 146573.
- [12] M.K. McKinney, B.F. Cravatt, Structure and function of fatty acid amide hydrolase, *Annu. Rev. Biochem.* 74 (2005) 411–432.
- [13] K. Ahn, D.S. Johnson, B.F. Cravatt, Fatty acid amide hydrolase as a potential therapeutic target for the treatment of pain and CNS disorders, *Exp. Opin. Drug Discov.* 4 (7) (2009) 763–784.
- [14] N. Clayton, et al., CB1 and CB2 cannabinoid receptors are implicated in inflammatory pain, *Pain* 96 (3) (2002) 253–260.
- [15] A.C. Howlett, M.E. Abood, CB(1) and CB(2) receptor pharmacology, *Adv. Pharmacol.* 80 (2017) 169–206.
- [16] L. Booker, et al., The fatty acid amide hydrolase (FAAH) inhibitor PF-3845 acts in the nervous system to reverse LPS-induced tactile allodynia in mice, *Br. J. Pharmacol.* 165 (8) (2012) 2485–2496.
- [17] M.D. Jhaveri, et al., Analgesic effects of fatty acid amide hydrolase inhibition in a rat model of neuropathic pain, *J. Neurosci.* 26 (51) (2006) 13318–13327.
- [18] L.C. Chiou, S.S. Hu, Y.C. Ho, Targeting the cannabinoid system for pain relief? *Acta Anaesthesiol. Taiwanica* 51 (4) (2013) 161–170.
- [19] J.M. Teixeira, et al., Peripheral soluble epoxide hydrolase inhibition reduces hypernociception and inflammation in albumin-induced arthritis in temporomandibular joint of rats, *Int. Immunopharmacol.* 87 (2020) 106841.
- [20] C. Nozaki, A. Markert, A. Zimmer, Inhibition of FAAH reduces nitroglycerin-induced migraine-like pain and trigeminal neuronal hyperactivity in mice, *Eur. Neuropsychopharmacol.* 25 (8) (2015) 1388–1396.
- [21] R. Greco, et al., Effects of peripheral FAAH blockade on NTG-induced hyperalgesia—evaluation of URB937 in an animal model of migraine, *Cephalalgia* 35 (12) (2015) 1065–1076.
- [22] R. Greco, et al., FAAH inhibition as a preventive treatment for migraine: a pre-clinical study, *Neurobiol. Dis.* 134 (2020) 104624.
- [23] O. Sasso, et al., Peripheral FAAH and soluble epoxide hydrolase inhibitors are synergistically antinociceptive, *Pharmacol. Res.* 97 (2015) 7–15.
- [24] J. Angelia, et al., Quinolinyln-based multitarget-directed ligands with soluble epoxide hydrolase and fatty acid amide hydrolase inhibitory activities: synthetic studies and pharmacological evaluations, *Heliyon* 10 (11) (2024) e32262.
- [25] S. Wilt, et al., Development of multitarget inhibitors for the treatment of pain: design, synthesis, biological evaluation and molecular modeling studies, *Bioorg. Chem.* 103 (2020) 104165.
- [26] S. Wilt, et al., Further exploration of the structure-activity relationship of dual soluble epoxide hydrolase/fatty acid amide hydrolase inhibitors, *Bioorg. Med. Chem.* 51 (2021) 116507.
- [27] C. Yuan, et al., Structure-activity relationship studies and pharmacological evaluation of 4-phenylthiazoles as dual soluble epoxide hydrolase/fatty acid amide hydrolase inhibitors, *Bioorg. Med. Chem.* 121 (2025) 118112.
- [28] J. Angelia, et al., Structure-activity relationship studies of benzothiazole-phenyl analogs as multi-target ligands to alleviate pain without affecting normal behavior, *Prostag. Other Lipid Mediat.* 164 (2023) 106702.
- [29] D. Carr, et al., 4-Phenyl-thiazole-based dual inhibitors of fatty acid amide hydrolase and soluble epoxide hydrolase do not alleviate orofacial inflammatory pain in female rats, *BBA Adv* 6 (2024) 100119.
- [30] S.S. Negus, et al., Preclinical assessment of candidate analgesic drugs: recent advances and future challenges, *J. Pharmacol. Exp. Ther.* 319 (2) (2006) 507–514.
- [31] R. Kandasamy, M.M. Morgan, 'Reinventing the wheel' to advance the development of pain therapeutics, *Behav. Pharmacol.* 32 (2&3) (2021) 142–152.
- [32] S. Mannix, et al., Measuring the impact of migraine for evaluating outcomes of preventive treatments for migraine headaches, *Health Qual Life Outcomes* 14 (1) (2016) 143.
- [33] J.M. Zakrzewska, et al., Evaluating the impact of trigeminal neuralgia, *Pain* 158 (6) (2017) 1166–1174.
- [34] H. Huang, et al., Development of highly sensitive fluorescent assays for fatty acid amide hydrolase, *Anal. Biochem.* 363 (1) (2007) 12–21.
- [35] P.D. Jones, et al., Fluorescent substrates for soluble epoxide hydrolase and application to inhibition studies, *Anal. Biochem.* 343 (1) (2005) 66–75.
- [36] S. Pecic, et al., Novel piperidine-derived amide sEH inhibitors as mediators of lipid metabolism with improved stability, *Prostag. Other Lipid Mediat.* 136 (2018) 90–95.
- [37] S. Pecic, et al., Synthesis and structure-activity relationship of piperidine-derived non-urea soluble epoxide hydrolase inhibitors, *Bioorg. Med. Chem. Lett* 23 (2) (2013) 417–421.
- [38] B. Haggman-Henrikson, et al., Increasing gender differences in the prevalence and chronification of orofacial pain in the population, *Pain* 161 (8) (2020) 1768–1775.
- [39] D.M. Lopes, et al., A refinement to the formalin test in mice, *F1000Res* 8 (2019) 891.
- [40] P. Clavelou, et al., Application of the formalin test to the study of orofacial pain in the rat, *Neurosci. Lett.* 103 (3) (1989) 349–353.
- [41] P. Raboisson, R. Dalle, The orofacial formalin test, *Neurosci. Biobehav. Rev.* 28 (2) (2004) 219–226.
- [42] C. Demartini, et al., Modelling migraine-related features in the nitroglycerin animal model: trigeminal hyperalgesia is associated with affective status and motor behavior, *Physiol. Behav.* 256 (2022) 113956.
- [43] R. Kandasamy, J.J. Calsbeek, M.M. Morgan, Home cage wheel running is an objective and clinically relevant method to assess inflammatory pain in male and female rats, *J. Neurosci. Methods* 263 (2016) 115–122.
- [44] J. Angelia, et al., Quinolinyln-based multitarget-directed ligands with soluble epoxide hydrolase and fatty acid amide hydrolase inhibitory activities: synthetic studies and pharmacological evaluations, *Heliyon* 10 (11) (2024) e32262.
- [45] K. Ahn, et al., Discovery and characterization of a highly selective FAAH inhibitor that reduces inflammatory pain, *Chem. Biol.* 16 (4) (2009) 411–420.
- [46] X. Wang, et al., Synthesis and evaluation of benzothiazole-based analogues as novel, potent, and selective fatty acid amide hydrolase inhibitors, *J. Med. Chem.* 52 (1) (2009) 170–180.
- [47] S.D. Kodani, et al., Design and potency of dual soluble epoxide hydrolase/fatty acid amide hydrolase inhibitors, *ACS Omega* 3 (10) (2018) 14076–14086.
- [48] B.D. Hammock, et al., Movement to the clinic of soluble epoxide hydrolase inhibitor EC5026 as an analgesic for neuropathic pain and for use as a nonaddictive opioid alternative, *J. Med. Chem.* 64 (4) (2021) 1856–1872.

- [49] S.H. Hwang, et al., Orally bioavailable potent soluble epoxide hydrolase inhibitors, *J. Med. Chem.* 50 (16) (2007) 3825–3840.
- [50] J. Besnard, et al., Automated design of ligands to polypharmacological profiles, *Nature* 492 (7428) (2012) 215–220.
- [51] M. Aggarwal, V. Puri, S. Puri, Serotonin and CGRP in migraine, *Ann. Neurosci.* 19 (2) (2012) 88–94.
- [52] X. Min, et al., Discovery and molecular basis of potent noncovalent inhibitors of fatty acid amide hydrolase (FAAH), *Proc. Natl. Acad. Sci.* 108 (18) (2011) 7379–7384.
- [53] S.R. Wilt, et al., Design, microwave-assisted synthesis, biological evaluation and molecular modeling studies of 4-phenylthiazoles as potent fatty acid amide hydrolase inhibitors, *Chem. Biol. Drug Des.* 95 (5) (2020) 534–547.
- [54] R. Abagyan, M. Totrov, D. Kuznetsov, ICM—a new method for protein modeling and design: applications to docking and structure prediction from the distorted native conformation, *J. Comput. Chem.* 15 (5) (1994) 488–506.
- [55] P. Sureda-Gibert, M. Romero-Reyes, S. Akerman, Nitroglycerin as a model of migraine: clinical and preclinical review, *Neurobiol. Pain* 12 (2022) 100105.
- [56] C. Tassorelli, et al., Nitroglycerin induces hyperalgesia in rats—a time-course study, *Eur. J. Pharmacol.* 464 (2–3) (2003) 159–162.
- [57] R. Greco, et al., Characterization of the peripheral FAAH inhibitor, URB937, in animal models of acute and chronic migraine, *Neurobiol. Dis.* 147 (2021) 105157.
- [58] S. Akerman, et al., Nitroglycerine triggers triptan-responsive cranial allodynia and trigeminal neuronal hypersensitivity, *Brain* 142 (1) (2019) 103–119.
- [59] R. Greco, et al., Effects of kynurenic acid analogue 1 (KYNA-A1) in nitroglycerin-induced hyperalgesia: targets and anti-migraine mechanisms, *Cephalalgia* 37 (13) (2017) 1272–1284.
- [60] R. Tarkany Basting, et al., Soluble epoxide hydrolase inhibitor blockage microglial cell activation in subnucleus caudalis in a persistent model of arthritis, *Int. Immunopharmacol.* 120 (2023) 110320.
- [61] H.B. Abdalla, et al., Soluble epoxide hydrolase inhibition avoid formalin-induced inflammatory hyperalgesia in the temporomandibular joint, *Inflammopharmacology* 30 (3) (2022) 981–990.
- [62] S.H. Pedersen, et al., Mechanisms of glyceryl trinitrate provoked mast cell degranulation, *Cephalalgia* 35 (14) (2015) 1287–1297.
- [63] R. Greco, et al., Effects of the dual FAAH/MAGL inhibitor AKU-005 on trigeminal hyperalgesia in male rats, *Cells* 13 (10) (2024).
- [64] C. Brenneis, et al., Soluble epoxide hydrolase limits mechanical hyperalgesia during inflammation, *Mol. Pain* 7 (2011) 78.
- [65] Y. Bu, et al., Role of soluble epoxide hydrolase in pain and depression comorbidity, *Neurobiol. Dis.* 193 (2024) 106443.
- [66] R. Kandasamy, et al., *Anti-migraine effect of Δ^9 -tetrahydrocannabinol in the female rat*, *Eur. J. Pharmacol.* 818 (2018) 271–277.
- [67] R. Kandasamy, et al., *Medication overuse headache following repeated morphine, but not Δ^9 -tetrahydrocannabinol administration in the female rat*, *Behav. Pharmacol.* 29 (5) (2018) 469–472.
- [68] R. Kandasamy, A.T. Lee, M.M. Morgan, Depression of home cage wheel running: a reliable and clinically relevant method to assess migraine pain in rats, *J. Headache Pain* 18 (1) (2017) 5.